Deep-Sea Research Part I 136 (2018) 107–118

Contents lists available at ScienceDirect

Deep-Sea Research Part I

journal homepage: www.elsevier.com/locate/dsri

Optically-derived estimates of phytoplankton size class and taxonomic group biomass in the Eastern Subarctic Pacific Ocean

Chen Zeng[a,b,*], Sarah Z. Rosengard[a], William Burt[a], M. Angelica Peña[c], Nina Nemcek[c], Tao Zeng[d,e], Kevin R. Arrigo[f], Philippe D. Tortell[a,g,h]

[a] Department of Earth Ocean and Atmospheric Sciences, University of British Columbia, 2207 Main Mall, Vancouver, BC, Canada V6T 1Z4
[b] School of Ocean and Earth Science, Tongji University, 1239 Siping Road, Shanghai 200092, China
[c] Institute of Ocean Sciences, Fisheries and Oceans Canada, P.O. Box 6000, Sidney, BC, Canada V8L 4B2
[d] National Satellite Ocean Application Service State Oceanic Administration, Beijing 100081, China
[e] Key Laboratory of Space Ocean Remote Sensing and Application State Oceanic Administration, Beijing 100081, China
[f] Department of Earth System Science, Stanford University, Stanford, CA 94305, USA
[g] Department of Botany, University of British Columbia, 1461-6270 University Boulevard, Vancouver, BC, Canada V6T 1Z4
[h] Peter Wall Institute for Advanced Studies University of British Columbia, 6331 Crescent Rd., Vancouver, BC, Canada V6T 1Z2

ARTICLE INFO

Keywords:
Particle absorption
Phytoplankton functional type
Photosynthetic pigments
Phytoplankton size class
Optics
Northeast Pacific Ocean

ABSTRACT

We evaluate several algorithms for the estimation of phytoplankton size class (PSC) and functional type (PFT) biomass from ship-based optical measurements in the Subarctic Northeast Pacific Ocean. Using underway measurements of particulate absorption and backscatter in surface waters, we derived estimates of PSC/PFT based on chlorophyll-a concentrations (Chl-a), particulate absorption spectra and the wavelength dependence of particulate backscatter. Optically-derived [Chl-a] and phytoplankton absorption measurements were validated against discrete calibration samples, while the derived PSC/PFT estimates were validated using size-fractionated Chl-a measurements and HPLC analysis of diagnostic photosynthetic pigments (DPA). Our results showflo that PSC/PFT algorithms based on [Chl-a] and particulate absorption spectra performed significantly better than the backscatter slope approach. These two more successful algorithms yielded estimates of phytoplankton size classes that agreed well with HPLC-derived DPA estimates (RMSE = 12.9%, and 16.6%, respectively) across a range of hydrographic and productivity regimes. Moreover, the [Chl-a] algorithm produced PSC estimates that agreed well with size-fractionated [Chl-a] measurements, and estimates of the biomass of specific phytoplankton groups that were consistent with values derived from HPLC. Based on these results, we suggest that simple [Chl-a] measurements should be more fully exploited to improve the classification of phytoplankton assemblages in the Northeast Pacific Ocean.

1. Introduction

Marine phytoplankton play a central role in ocean ecology and global carbon cycling (Caddy et al., 1995; Parsons and Lalli, 2002). On an annual basis, these microscopic organisms convert approximately 50 GT of CO_2 into organic matter (Siegenthaler and Sarmiento, 1993), supporting nearly all marine upper trophic level biomass, and contributing substantially to the oceanic uptake of atmospheric CO_2 through the biological carbon pump. Understanding the quantitative significance of phytoplankton to ocean ecology and biogeochemical cycling requires information on total biomass, as well as the relative biomass of different phytoplankton size classes (PSCs) and functional types (PFTs). These PSCs/PFTs categorize phytoplankton assemblages based on various characteristics including cell size, and physiological and metabolic attributes.

By definition, different PSCs/PFTs contribute in unique ways to ocean ecology and biogeochemical cycles. For example, differences in cell size and the presence of mineral-phase shells in some groups (e.g. diatoms and some coccolithophores) influence phytoplankton sinking rates and their contribution to vertical carbon fluxes (Armstrong et al., 2002; Buesseler, 1998; Francois et al., 2002; Klaas and Archer, 2002; Michaels, 1988). In addition, certain phytoplankton groups play specific roles in elemental cycles through nitrogen fixation (many cyanobacteria), elevated production of dimethyl sulfide (many prymnesiophytes, silicoflagellates and dinoflagellates), and the uptake of silicic acid (all diatoms). Classification of a phytoplankton assemblage into

* Corresponding author at: Department of Earth Ocean and Atmospheric Sciences, University of British Columbia, 2207 Main Mall, Vancouver, BC, Canada V6T 1Z4.
E-mail address: 07zengchen@tongji.edu.cn (C. Zeng).

https://doi.org/10.1016/j.dsr.2018.04.001
Received 1 November 2017; Received in revised form 31 January 2018; Accepted 3 April 2018
Available online 04 April 2018
0967-0637/

PSCs/PFTs can also shed light on carbon uptake capacity (Platt and Denman, 1977) and different nutrient and light requirements for growth (Aiken et al., 2008; Bouman et al., 2005; Platt et al., 2005). For example, large phytoplankton with low surface area to volume ratios (e.g. many diatoms) require nutrient-rich water to sustain active growth, while smaller pico-phytoplankton (e.g. *Synechococcus* and *Prochlorococcus*) have higher surface area to volume ratios and more efficient nutrient uptake mechanisms, enabling them to thrive in oligotrophic regions (Waterbury et al., 1979; Zubkov et al., 2003).

In some instances, there may be a good correspondence between taxonomic and PFT classifications. For example, calcifying phytoplankton groups are mostly represented within the Prymnesiophyte class, whereas silicon cycling is associated specifically with diatoms. For this reason, estimation of PFTs has often been linked to an analysis of phytoplankton taxonomic composition. Traditionally, estimates of phytoplankton community composition relied on analysis of discrete water samples using microscopy (e.g.,Booth et al., 1993). This approach can provide unambiguous information on phytoplankton assemblage taxonomy down to the species level. However, the method is time consuming and requires significant expertise, and the identification of phytoplankton species by light microscopy is challenging in regions dominated by smaller cell assemblages (e.g. pico-eukaryotes). To circumvent these problems, there has been increasing use of high performance liquid chromatography (HPLC) for the analysis of accessory photosynthetic pigments as diagnostic indicators of certain phytoplankton groups (Uitz et al., 2006; Vidussi et al., 2001). Two major analysis schemes have been developed to identify taxonomic composition based on a matrix of pigment concentrations (CHEMTAX, (Mackey et al., 1996) and diagnostic pigment analysis (DPA), (Hirata et al., 2011a; Uitz et al., 2006; Vidussi et al., 2001)). Note that the original DPA analysis developed by Vidussi et al (2001) and revised by Uitz et al. (2006) was developed for estimating phytoplankton size classes, not taxonomic groups. Hirata et al. (2011b) interpreted the DPA for identification of phytoplankton groups, but these authors did not present independent microscopy or molecular data to validate their derived taxonomic abundance estimates. While HPLC data are potentially advantageous over microscopy for studying phytoplankton composition, there are uncertainties and limitations with HPLC data, as pigment concentrations are sensitive to environmental conditions (e. g. light and nutrient supply) (Obayashi et al., 2001).

In recent years, there has been increasing interest in automated methods to estimate PSC/PFT abundance/biomass from ship-board cell counting/imaging, and from optical measurements. For example, ship-board imaging flow cytometers (e.g. FlowCAM) can optically measure size and shape attributes of individual cells, while providing digital microscopic images for taxonomic identification. This method has been used with some success (Zubkov et al., 2000, 2003), but sample analysis requires deep learning algorithms with extensive training reference libraries, and is restricted to pico- and nano- planktonton groups. Another approach is based on the measurement of seawater inherent optical properties (IOPs) to quantify absorption and backscattering coefficients across multiple wavelengths. These observations can provide insight into the composition of phytoplankton assemblages and particle size distributions, based on taxonomic and size-dependent effects on light absorption and backscatter spectra (Ciotti et al., 2002; Kostadinov et al., 2009; Lin et al., 2014; Organelli et al., 2013; Xi et al., 2015; Zhang et al., 2015). The measurements can be collected from flow-through systems (Slade et al., 2010), moorings (Bélanger et al., 2013; Twardowski et al., 2007), satellites and aircraft (Alvain et al., 2005; Kostadinov et al., 2009; Uitz et al., 2006), enabling observations over a large range of spatial and temporal scales.

In this article, we examine the utility of IOP measurements to provide information on PSCs/PFTs in the Subarctic Pacific Ocean. This region is characterized by contrasting hydrographic and productivity regimes, from iron-limited HNLC offshore waters to high productivity coastal upwelling regimes. Significant research has been conducted to examine the spatial and temporal variability of phytoplankton biomass and productivity in this region (Harrison et al., 2004, 1999), as well as the taxonomic composition of phytoplankton assemblages based on microscopy (Booth et al., 1993; Peña and Varela, 2007). To our knowledge, however, there has been no attempt to use IOP measurements to examine phytoplankton taxonomy and PSCs/PFTs in the Subarctic North Pacific. Such an approach, if validated, would be of significant benefit in understanding ecosystem variability in this region and its response to environmental forcing. Our objective was to collect new observations of seawater IOPs across a range of hydrographic and productivity regimes in the Subarctic Pacific, and to compare several existing algorithms for PSCs/PFTs determination against size-fractionated [Chl-a] measurements and HPLC analysis of accessory photosynthetic pigments.

2. Methods

2.1. Underway optical measurements

Seawater optical properties were measured on three oceanographic cruises conducted during spring and summer, 2016. The Line P and La Perouse cruises were conducted on the *CCGS John P. Tully* during May/June, while a third expedition was conducted in July on the *R/V Oceanus*. The cruise tracks (Fig. 1) covered a range of hydrographic and productivity regimes in the northeast Subarctic Pacific Ocean.

We used the same ship-board underway analysis system on all three cruises. The system was operated autonomously, with custom LabVIEW software (National Instruments) used to run all aspects of system control and data acquisition, including GPS position information. Optical measurements were derived from an underway flow-through system, which sampled a continuous surface (~ 5 m) seawater supply through various sensors. Flowing seawater (5 L min^{-1}) was passed through a debubbler prior to analysis by a WETLabs ECO-BB3 meter to measure backscattering at 117° at 3 wavelengths (470, 532 and 650 nm) (Dall'Olmo et al., 2012), followed by a WetLabs AC-s to measure absorption and attenuation at 83 wavelengths between 400 nm and 740 nm. Raw data derived from the BB3 and AC-s were treated in MatLab to derive estimates of phytoplankton absorption and particulate backscatter (see below). All underway measurements were averaged into 1 min sampling bins along the cruise tracks.

We removed the contribution of dissolved seawater constituents to the measured AC-s absorption signal. To do this, an automated 3-way valve redirected sample water through in-line 1 μm and 0.2 μm pore-size filters for 10 min out of every 70 min of continuous seawater measurements. The filtrate provided a measure of the optical properties of dissolved constituents, and this value was subtracted from our measurements to isolate the particulate absorption (a_p) signal. Following the approach of (Slade et al., 2010), a_p was adjusted by spectrum discontinuity and residual temperature corrections using Matlab function *fminsearch*. The latter correction is based on the positive correlation between water temperature and absorption at 470 nm. All details for this correction can be found in WebLab AC-s user manual (http://www.seabird.com/sites/default/files/documents/acsm.pdf).

The BB3 sensor was installed in a custom-built dark acrylic chamber with a volume of 4 L. Following the method described by (Dall'Olmo et al., 2012), we measured particulate backscatter at 470, 532, 650 nm using the BB3 sensor. Dark counts (D) and wall effects ($b_{b,wall}$) from the chamber were measured as described by Burt et al. (2018) and subtracted from the measured sample counts (C). A scale ratio from factory calibration of the BB3 instrument was used to convert the corrected digital counts to the volume scattering function (m^{-1}) (S) and an angle-specific *chi* factor (an χ_p factor of 1.1 relating to the volume scattering function at 117°to b_{bp}) was applied to estimate particulate backscattering (b_{bp}) (Dall'Olmo et al., 2012) (Fig. 2).

$$b_{bp} = 2\pi\chi_p [S(C - D) - \beta_{SW}] - b_{b,wall} \quad (1)$$

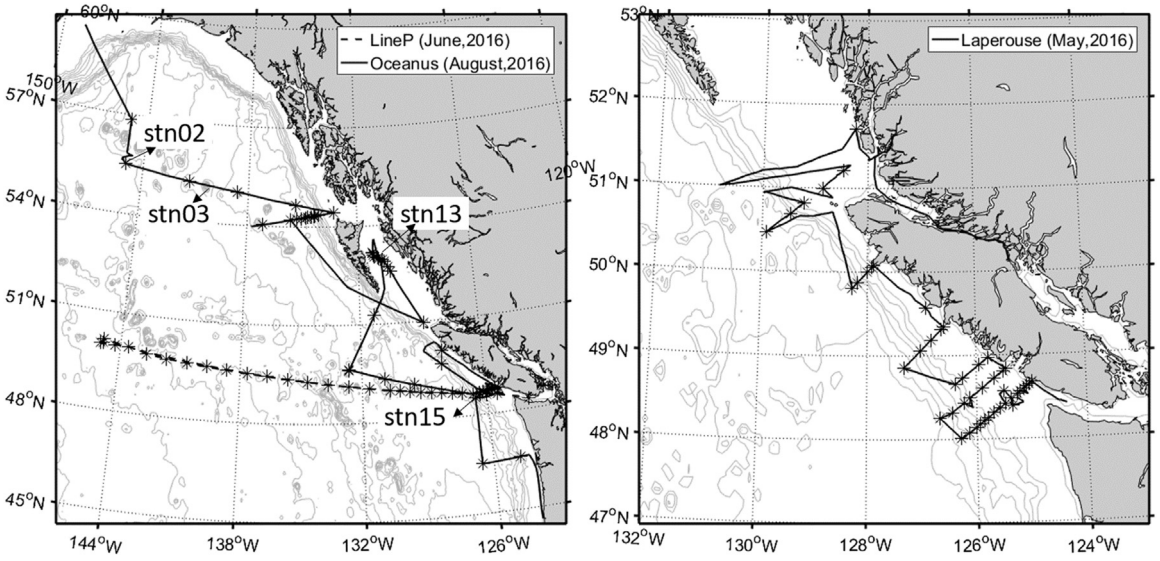

Fig. 1. Cruise map for the Line P and Oceanus cruises (a), and the La Perouse cruise (b). Stations identified with numbers show the locations where discrete samples for absorption spectra were collected. Asterisks denote stations where discrete HPLC and fluorescence [Chl-a] samples were collected for calibrations of [Chl-a] line height estimation and DPA analysis.

2.2. *In situ Chl-a and a_{ph} measurements*

The robustness of the PFT/PSC classification approach described below depends upon the capability of continuous flow-through measurements to accurately quantify surface ocean optical properties. To assess this, we compared a suite of properties derived from discrete calibration samples against underway optical measurements obtained within 5 min of the discrete sample collection times (Fig. 3).

2.2.1. *Underway Chl-a estimation*

Continuous underway measurements of [Chl-a] were derived from

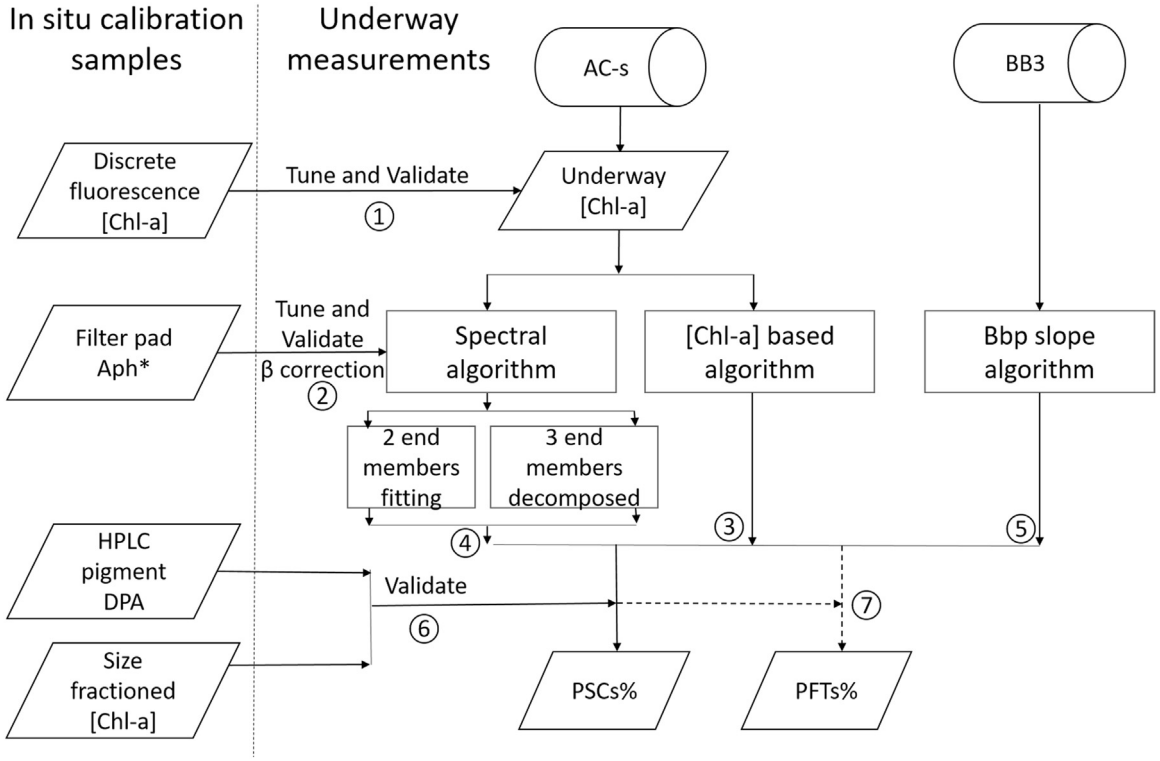

Fig. 2. Flowchart of the method used to tune and validate ship-board underway measurements. Step 1 involved the regional tuning and validation of the relationship between discrete [Chl-a] and absorption line height (a_p^{LH}), measured from all three summer 2016 cruises (n = 85). Step 2 is the tuning and validation of phytoplankton absorption (a_{ph}*) values from the Zhang et al. (2013) inversion with filter pad-based a_{ph}* collected on the Oceanus cruise. Steps 3, 4, and 5 are estimates of micro%, nano% and pico% (fraction of phytoplankton > 20 μm, 2–20 μm and < 2 μm) using three algorithms described in Section 2.3. Steps 6 and 7 are validations of underway PSCs% and PFTs% estimates, derived from the three algorithms, against HPLC-derived diagnostic pigment analysis (DPA) based on Hirata et al. (2011b). For this validation, we used HPLC measurements collected on the Oceanus cruise (n = 65) and, also measurements of discrete [Chl-a] (via discrete fluorescence analysis) and HPLC-based DPA from historical Line P cruises (2007–2011, n = 43).

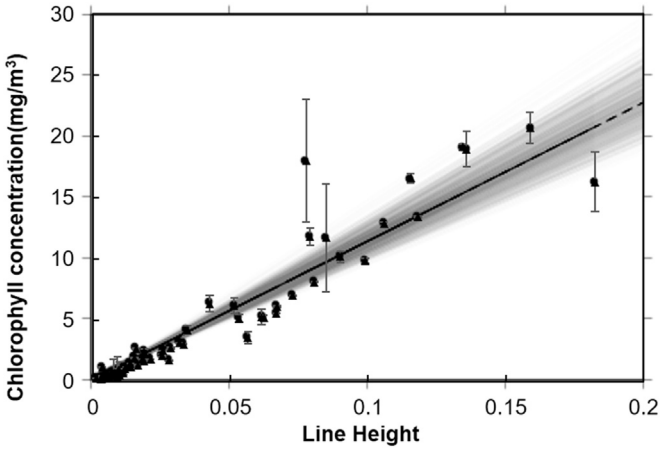

Fig. 3. Power law regression between line height of a_p 676 nm and discrete fluorescence [Chl-a], r2 = 0.95, RMSE between measured and predicted [Chl-a] is 0.16 mg/m^3. Grey lines denote the results of 1000 boot-strap analyses, used to define the uncertainty of this approach.

the 676 nm absorption line height (a_p^{LH}) approach developed by (Roesler and Barnard, 2013). This absorption peak is believed to have no significant contribution from non-algal particles (NAP), thus providing a proxy for [Chl-a]. We derived a regional relationship between underway a_p^{LH} measurements and [Chl-a] by regressing underway measurements against 138 discrete [Chl-a] measurements collected from Niskin bottle casts (5 m depth) during the three cruises. For these discrete measurements, duplicate 500 mL samples were filtered under low vacuum (< 15 kpa) onto 0.7 μm Whatman GF/F filters, and stored in a − 80 °C freezer until subsequent analysis within several days. Prior to analysis, filters were immersed in 90% acetone overnight at − 20 °C to extract [Chl-a]. The extracts were analyzed using fluorometry (10-AU Fluorometer, Turner) before and after the addition of 10% HCl to estimate Chl-a and phaeophytin-a concentrations, respectively. Duplicate measurements with a relative measurement error less than 10% of the mean were used for this validation exercise. These discrete [Chl-a] measurements were compared to average a_p^{LH} values obtained within a ± 5 min interval of sample bottle closure at discrete sampling stations. This match up resulted 85 paired measurements for comparison. Some discrete validation points could not be used, as they coincided with periods when system filters were being changed on station, or during periods of automated blank measurements.

In follow up cruises to the Subarctic Pacific during summer 2017, we also collected discrete measurements of size-fractioned [Chl-a] to validate PSC estimates. These cruises were conducted on the *John P. Tully* and *Oceanus*, following cruise tracks similar to those described above for our 2016 work. For this analysis, we filtered 500 mL of water through 3 stacked polycarbonate filters (20, 2 and 0.2 μm) separated by mesh spacer disks. The filters were treated as described above for fluorescence [Chl-a] measurements, and the resulting data used to estimate the fraction of total phytoplankton biomass in the three different size classes.

2.2.2. Filter pad a_{ph} measurements

Phytoplankton absorption (a_{ph}) spectra in discrete calibration samples were measured spectrophotometrically using the filter pad approach described by (Mitchell, 1990; Pegau et al., 2002). For these measurements, 500 mL of seawater were filtered onto triplicate 25 mm GF/F filters at every station during the Oceanus Cruise. All filters were immediately frozen in liquid nitrogen and stored at − 80 °C before analysis by spectrophotometry (100 Bio UV–Visible Spectrophotometer, Cary).

Filters were measured once to obtain the total particulate absorption (a_p) spectrum, which includes contributions from phytoplankton and non-algal particles (a_{NAP}), and measured again following an extraction in 90% methanol to remove pigments from the sample. The spectrum obtained in the methanol-extracted samples represents the contribution of non-algal particles (NAP, i.e. detritus) to absorption, and this is subtracted from the total particulate signal to obtain an estimate of phytoplankton-specific digital counts (D_{ph}). This value was converted to a_{ph} following *Mitchell et al.* [1990]:

$$a_{ph}(\lambda) = 2.303[D_{ph}(\lambda)]\frac{A_{eff}}{\beta V_{filt}} \quad (2)$$

$$\beta(\lambda) = 2.2536 D_{ph}(\lambda)^{0.0738} \quad (3)$$

$$\lambda \in [400, \quad 700]$$

where A_{eff} is the effective area of the filter pad (m^2) and V_{filt} (m^3) is the volume of the sample filtered, λ is band wavelength. These measurements are spectrally dependent, but the wavelength-dependence term, λ, will be omitted from the remainder of the paper in the interest of brevity. The empirical β value corrects for the difference in the path length through the sample on a filter pad versus a sample in suspension (Bricaud and Stramski, 1990). The coefficients used to estimate β are based on Eqs. (2) and (3) derived from the optimal fit between underway a_{ph} values from AC-s measurements and filter-pad D_{ph}. Previous work has shown that the filter-pad a_{ph} values calculated using this power-law β correction better match a_{ph} values derived from AC-s measurements (Slade et al., 2010). In our case, applying the β correction to the filter pad a_{ph} adjusted the absolute values by < 7% at all visible wavelengths (400–700 nm), leaving the spectral shapes largely unchanged.

2.2.3. HPLC measurements and diagnostic pigment analysis

We used HPLC measurements to quantify the concentration of various accessory phytoplankton pigments. Discrete samples for pigment analysis (1 L) were collected on the Oceanus cruise. Samples were filtered onto GF/F filters, flash frozen in liquid nitrogen and stored at − 80 °C until analysis within several months. Samples (n = 65) were analyzed at the NASA Goddard Space Flight Center Ocean Ecology Laboratory (Van Heukelem and Thomas, 2001). We also obtained additional archived HPLC data (n = 43) from Line P cruises between 2007 and 2011 (Nemcek and Pena, 2014).

We used DPA of the HPLC data to derive estimates of the size structure and taxonomic composition of phytoplankton assemblages in the discrete samples. The size classes approach, initially developed by (Vidussi et al., 2001) and refined by (Uitz et al., 2006), classifies phytoplankton group biomass based on the relative concentration of certain diagnostic pigments (DP) normalized to total [Chl-a]. Following the model of Hirata et al. (2011b), we applied this DPA approach to estimate the relative biomass of six phytoplankton groups (diatoms, dinoflagellates, prymnesiophytes, chlorophytes, pico-eukaryotes, and prokaryotes) and three phytoplankton size classes, micro-phytoplankton (> 20 μm diameter), nano-phytoplankton (2–20 μm diameter) and pico-phytoplankton (< 2 μm diameter). These DPA-based estimates were used to validate optically-derived estimates of PSCs/PFTs (see Table 1).

In addition to the validation measurements we conducted on our cruises, we also used data from the Line P program data archive to examine the relationship between Chl-a concentrations and PSCs/PFTs. These historical data were derived from the same Line P stations shown in Fig. 1, and include discrete measurements of fluorescence-based [Chl-a] concentrations, and HPLC measurements of photosynthetic pigments to validate the [Chl-a] based approach in NP.

2.3. Optical estimates of phytoplankton functional groups

We compared the ability of four different algorithms to estimate the fraction of different phytoplankton size classes in the surface water

Table 1
Coefficients and formula on estimating PSCs/PFTs.

PSCs/PFTs	DPA model	[Chl-a] based approach[b]
Micro-plankton	1.41(Fuco + Perid)/$\sum DP$[a]	$[0.9117+\exp(-2.733x+0.4003)]^{-1}$
Nano-plankton	(0.5 *1.27Hex + 1.01Chl-b + 0.35But + 0.6Allo)/ $\sum DP$[a]	1-Micro-Nano
Pico-plankton	(0.86Zea + 0.5 *1.27Hex)/ $\sum DP$[a]	$-[0.1529+\exp(1.0306x-1.5576)]^{-1} - 1.8597x + 2.9954$
Diatom	1.41Fuco/$\sum DP$[a]	nkton size classes in the surface water ass
Dinoflagellate	1.41Perid/$\sum DP$[a]	Micro-Diatom
Chlorophyte	1.01Chl-b/ $\sum DP$[a]	$(0.249/y)\exp[-1.2621(x-0.5523)^2]$
Prymnesiophytes	(0.5 *1.27Hex + 0.35But + 0.6Allo)/ $\sum DP$[a]	Nano- Chlorophyte
Prokaryotes	0.86Zea/ $\sum DP$[a]	$\left(\frac{\frac{0.0067}{0.6154}}{y}\right)\exp\left[-\frac{19.519(x-1.8597)^2}{0.6154^2}\right]$ $+0.1027x^2 - 0.1189x + 0.0626$
Pico-eukaryotes	0.5 * 1.27Hex/ $\sum DP$[a]	Pico - Prokaryotes

[a] $\sum DP$ = 1.41Fucoxanthin (Fuco) + 1.41Peridinin (Perid) + 1.27 19'-Hexanoyloxyfucoxanthin (Hex) + 0.6Alloxanthin (Allo) + 0.35Butanoyloxyfucoxanthin (But) + 1.01Chlorophyll-b (Chl-b) + 0.86 Zeaxanthin (Zea) = Chl-a.
[b] $x = log_{10}(Chl-a); y = Chl-a$.

assemblages (Fig. 2). These algorithms were the [Chl-a] based algorithm (Hirata et al., 2011b), the two end-member spectral fitting algorithm (Zhang et al., 2013), three end-member spectral decomposition algorithm (Zhang et al., 2015) and the backscatter slope algorithm (Kostadinov et al., 2009). Applications of these algorithms are briefly described below, and readers are referred to the original publications for more detailed information.

2.3.1. Chl-a based approach

Hirata et al. (2011b) developed an algorithm to estimate PSCs/PFTs biomass based on the relationship between total [Chl-a] and HPLC-derived DPA from a global data set of observations. This approach is based on the relationship between PSC distributions and trophic status, with eutrophic waters ([Chl-a] > 1 mg/m^3) typically dominated by micro-phytoplankton such as diatoms, and oligotrophic waters ([Chl-a] < 0.1 mg/m^3) dominated by pico-phytoplankton (Zhang et al., 2015). We applied the algorithm of Hirata et al. (2011b) using our underway $[Chl\text{-}a]_{LH}$ measurements from all three cruise tracks. The PSC/PFT estimates derived from this approach were validated against estimates obtained using discrete HPLC measurements (Section 2.2.3). The relevant equations for this model are presented in Table 1.

2.3.2. Two end-member spectral fitting approach

Spectral response algorithms estimate PSCs/PFTs using the absorption spectra of different phytoplankton size classes (Zhang et al., 2015, 2013) inferred from laboratory measurements of mono-specific phytoplankton cultures (Ciotti et al., 2002; Uitz et al., 2008). Size-dependent differences in a_{ph} spectra result from both the unique pigmentation of different groups, and also from size-dependent pigment packaging effects (Bricaud et al., 2004). We used the spectral fitting approach of Ciotti et al. (2002) to estimate the fractional contribution of two phytoplankton end member groups, pico and micro-phytoplankton, to total a_{ph} from 400–700 nm (Zhang et al., 2013). We applied a non-linear fitting approach (Zhang et al., 2013) to separate the contributions of a_{ph} and a_{NAP} to total AC-s derived a_p, where a_{NAP} is an exponential function of wavelength, and a_{ph} is derived from the combination of two kernels, a^*_{micro} and a^*_{pico}.

$$a_p = [Chla]_{LH} \times a^*_{ph} + a_{NAP} \quad (4)$$

$$a^*_{ph} = c_1 \times a^*_{micro} + (1-c_1)\times a^*_{pico} \quad (5)$$

$$a_{NAP} = c_2 e^{-c_3(\lambda-400)} \quad (6)$$

In Eqs. (4) and (5), a^*_{ph} is a_{ph} normalized to [Chl-a]. The input kernels a^*_{micro}, a^*_{pico} used in our fitting procedure were obtained from Ciotti et al. (2002) who derived a^*_{ph} from size fractioned samples. We applied a constrained nonlinear estimation using the Matlab function fmincon to approximate coefficients c_1, c_2 and c_3 based on an absolute value penalty function. The range for each unknown c_1, c_2 and c_3 were based on published values (Zhang et al., 2013).

2.3.3. Three end-member spectral decomposition approach

In more recent work, Zhang et al. (2015) modified their model into a three group PSCs estimation approach. This approach decomposed a_p into 4 kernels of a^*_{micro}, a^*_{nano},a^*_{pico} and based on Singular Value Decomposition (SVD). This decomposition inverted linear system combination of 4 kernels by regulating coefficient values within the range of [0, 1]. Those coefficients represent the relative contribution of micro-plankton, nano-plankton, pico-plankton and CDOM. The kernels of PSCs were provided from Utiz et al., 2008. The kernel of were shown as follows:

$$a_{CDOM}(\lambda) = a_{CDOM}(400)\exp(-0.011(\lambda-400)) \quad (7)$$

Where, − 0.011 denotes for the slope of CDOM they approached from two global datasets (Laboratoire d'Océanographie de Villefranche dataset and the NASA bio-Optical Marine Algorithm Dataset), and a time series dataset of coastal ocean (the Martha's Vineyard Coastal Observatory dataset).

2.3.4. Backscatter slope approach

Previous studies have shown that spectrally-resolved backscatter coefficients can be used to estimate phytoplankton cell sizes. Kostadinov et al. (2009) employed a Mie theory-based relationship between the b_{bp} slope and particle size distribution (PSD) to estimate pico-, nano-, and micro- size particle volumes and abundances. The b_{bp} coefficients we measured at the three BB3 wavelengths (479, 532, 650 nm) were fit to a wavelength-dependent exponential function to obtain a b_{bp} slope (η). We then used the look-up table of Kostadinov et al. (2009) to derive a unique particle size distribution slope (ξ) value for each measured value of η, allowing us to estimate the relative volumetric contribution of different particle size classes:

$$V = \frac{1}{4-\xi}\frac{\pi}{6}N_0 D_0^{\xi}(D_{max}^{4-\xi} - D_{min}^{4-\xi}) \quad (8)$$

where V is the particle volume in three size ranges, and D corresponds to three particulate diameter intervals, pico-(0.5–2 μm), nano-(2–20 μm) and micro-(20–200 μm) phytoplankton. Fractions of different size classes (e.g. micro-phytoplankton; micro%) were calculated by the volume ratio with the sum of all size classes (e.g. $V_{micro}/V_{pico+nano+micro}$).

2.4. Satellite matchups

The ocean color-derived [Chl-a] estimates were collected for satellite match ups, using the daily merged outputs from the OCI algorithm of AquaModis remote sensing reflectance data, with 4 km spatial resolution. We extracted the underway [Chl-a] located within each of the satellite pixels for each sampling day, resulting in 2080 paired match up data points for all three 2016 cruises. Mean and standard deviation were calculated for each underway [Chl-a] matching window. We removed all match up points where the in situ Chl measurements showed a relative standard deviation greater than 10%.

2.5. Error analysis

For Monte Carlo uncertainty estimation, we used the equations of Hirata et al. (2011b) (Table 1) to derive PFTs from a set of 10,000 normally distributed [Chl-a] values ranging from 0.1 to 10 mg/m^3. We examined the sensitivity of the calculations to ± 15% random noise added to [Chl-a]. Furthermore, we used the resulting PFTs estimates to derive concentrations of the various diagnostic pigments, by inverting the equations of Hirata et al. (2011b) (Table 1). These pigment estimates were, in turn, used to estimate PFTs using a DPA approach. We then re-computed the DPA results allowing either ± 5 or 15% random error in the pigment concentrations to examine the resulting effect on PFTs estimation. The resulting difference in the magnitude of each PSCs/PFTs was considered as the bias caused by the noise in the initial pigment composition assigned for each phytoplankton group.

3. Results

3.1. Tuning and validation of the underway measurements

The discrete sample data set collected over three cruises allowed for regional tuning and validation of absorption line height-based [Chl-a] measurements (a_p^{LH}), and AC-s derived phytoplankton absorption spectra (a_{ph}). Prior studies have documented a power law relationship between a_p^{LH} and [Chl-a], which results, in part, from phytoplankton pigment packaging (Nelson et al., 1993). In our data set, we also found a strong correlation between a_p^{LH} and discretely measured [Chl-a] in 85 underway match-ups. Best-fit coefficients yielded a predictive power-law relationship that explained 95% of the total variance (r^2 = 0.95) in [Chl-a], with an RMSE of 0.16 mg/m^3 (Eq. (2)). The model was fit using the cross-validation bootstrap method to calculate appropriate coefficients and estimates of RMSE for model validation. All coefficients and RMSEs from 1000 iterations were averaged for optimal output. Grey lines in Fig. 3 show the regression of all 1000 results and provide an estimate of the uncertainty of this approach, where higher [Chl-a] has higher uncertainties. Even in the most productive waters, with [Chl-a] higher than 20 mg/m^3, the relative uncertainty was smaller than 12% The strength of this relationship confirms the efficacy of using underway absorption line height as a measure of [Chl-a] in our study region.

$$[Chla]_{LH} = 132.8 a_p^{LH1.0906} \quad (9)$$

Underway measurements of a_{ph} compared well with discrete a_{ph} measured by the filter pad method (Fig. 4). For all sample matchups, the shoulders, peaks and slopes from both methods occurred at nearly identical wavelengths, with similar wavelength-dependent slopes. The similarity in spectral shapes between the discrete and underway measurements was quantitatively assessed by computing hyper-dimensional Euclidean distances between the two spectra. The results of this analysis showed that the maximum error was 0.05 m^{-1}, and the average error over all wavelengths (0.0003 m^{-1}) was less than 7% of the a_{ph}* signal. This matchup validates the use of the non-linear fitting function (Zhang et al., 2013) (Section 2.3.2) to differentiate a_{ph} from total a_p.

An abnormal feature around 580–600 nm of underway a_{ph}* was also apparent in our measurements, as a small drop in absorption (e.g see Fig. 4.c). There are three potential causes for this feature. Low phytoplankton absorption in this wavelength band resulted in weak signals that were vulnerable to measurement errors. Moreover, the AC-s instrument has a discontinuity within 580–600 since the two sensors converged at this wavelength at the outer limited of their measurement windows (~400 to ~590 nm and ~590 to ~750 nm, respectively). Finally, we applied residual temperature correction for approaching a_p and then a_{ph}*. The pure water temperature dependence used in this correction has a bump in around 600 nm (shown in Fig. 2.b of Slade et al., 2010), which could contribute the apparent drop in signal intensity. Although the exact cause of this signal anomaly is not clear, it has only a minor effect on our analyses.

Measurements of b_{bp} at wavelengths of 470, 532 and 650 nm had a range of 0.001–0.315 m^{-1}, 0.0006–0.028 m^{-1}, 0.0005–0.029 m^{-1}, respectively, while the wavelength-dependece of b_p (η) varied between − 1.5 and 2.9 m^{-1}. Following the work of (Kostadinov et al., 2009), we interpret this variability in terms of shifts in particle size distributions. Slopes were generally lower in eutrophic waters, indicating larger particles, whereas higher slopes in non-productive areas indicated lower mean particle sizes. As an example of this, Fig. 5 shows a sharp gradient in the back-scatter slope across a transition zone from low to high Chl-a (associated with a hydrographic frontal zone). These results were derived from a portion of the Line P cruise (from latitude 48.86°, longitude −129.23° to latitude 48.97° longitude −130.67°) in the vicinity of Vancouver Island, where we encountered a prominent hydrographic frontal feature caused by eddy (Burt et al., in press).

3.1.1. PSCs estimation based on four different phytoplankton size estimation algorithms

Estimates of PSCs derived using four different algorithms (Section 2.3) were compared against values derived from DPA analysis of discrete HPLC data (Fig. 6). The [Chl-a]-based approach showed the best match with HPLC-derived estimates, capturing 88%, 67% and 86% of the variation micro%, nano% and pico%, respectively (i.e. r2 = 0.88, 0.67 and 0.86). All of the other approaches, spectral fitting, spectral decomposed and b_{bp} slope approaches showed a poorer fit to the validation data. The two end-member spectral fitting approach produced the second best results, explaining more than 80% of the variance in micro% (r2 = 0.84 and RMSE = 0.12) and pico% (r2 = 0.82 and RMSE = 0.07). The three end-member spectral decomposition approach produced lower accuracy estimates, with r2 values of 0.51, 0.35 and 0.14 for pico%, micro% and nano%, respectively. The bbp slope approach was unable to explain more than one third of the variance in PSCs observed in HPLC-derived DPA analysis with r2 values of 0.31, 0.12 and 0.29 for micro%, nano% and pico%, respectively.

We further validated the PSCs-estimates derived from the Hirata et al. (2011b) model against discrete measurements of size-fractioned [Chl-a]. This validation was based on a set of observations made during summer 2017 cruises to the Subarctic Pacific Ocean (see methods). The results show good general agreement between the predicted and observed micro% (Fig. 7; r2 = 0.78, RMSE = 0.12,), with somewhat poorer agreement for nano% (r2 = 0.50, RMSE = 0.11) and pico% (r2 = 0.50, RMSE = 0.13). Most of the points fall within the 15% interval of the Hirata et al. (2011b) model, although there was a tendency to under-predict micro% and over-predict nano% at low Chl values. In addition, there were two obvious outliers, where the model significantly over-predicted micro% and under-predicted nano% relative to observed values (in the dashed circle of both figs). These two points were derived from measurements on the 2017 Oceanus cruise in the vicinity of an elevated calcite signal observed from satellite.

3.1.2. Estimation of PFTs biomass

In addition to providing estimates of phytoplankton size structure (i.e. micro%, nano% and pico%), the approach described by Hirata et al. (2011b) also yields estimates of the relative biomass of six

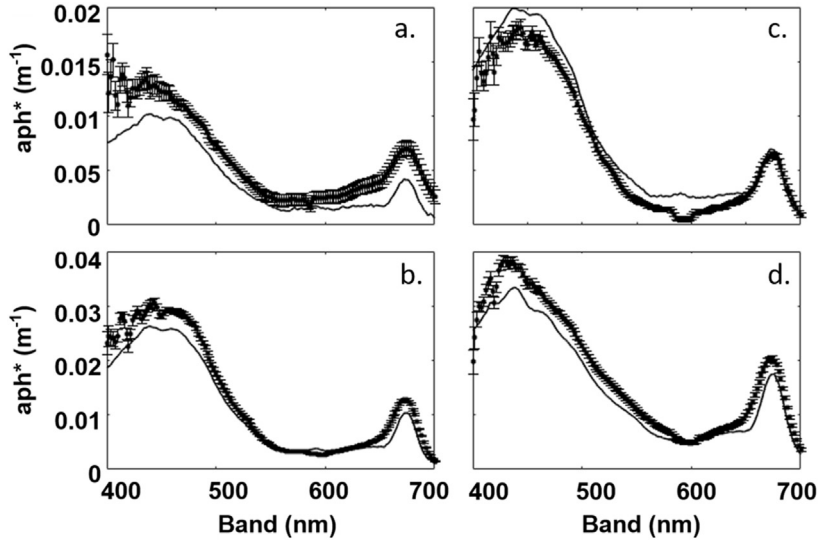

Fig. 4. Spectra of filter pad a_{ph}* (thin line) and AC-s-derived underway a_{ph}* (symbols with error bar) measured at a) stn02; b) stn03; c) stn13; d) stn15.

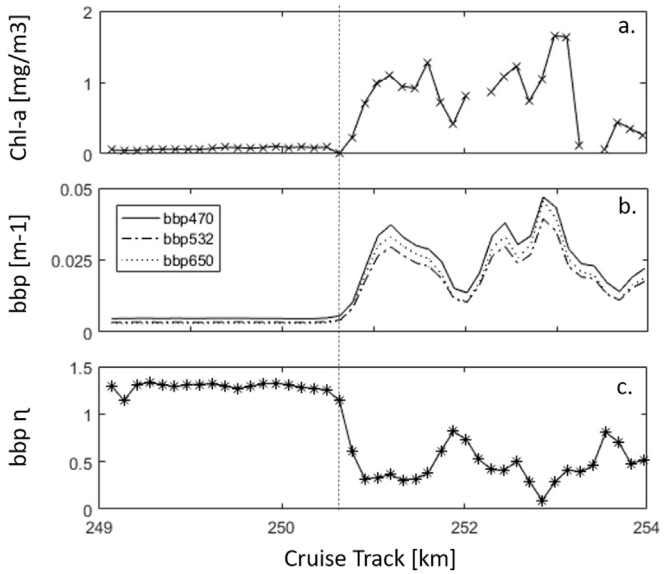

Fig. 5. Measurements of Chl-a concentration (a); b_{bp} coefficients from BB3 measurements at three wavelengths (b); and derived wavelength-dependence of b_{bp} (η) (c) along a short portion of the Line P cruise track from latitude 48.86°, longitude − 129.23° to latitude 48.97° longitude − 130.67°.

phytoplankton functional types from [Chl-a]. We found good agreement between relative biomass predicted by the Hirata et al. (2011b) model and those derived from DPA analysis of HPLC data from the Oceanus cruise and Line P data archive (Fig. 8). Despite a few outliers, the model prediction encapsulated nearly all of the DPA-based estimates to within ± 15%. Estimates of low biomass groups including chlorophyte and pico-eukaryotes deviated from pigment-based fractional contributions more than the other groups. Overall, we found that 79% of the variance in the relative biomass of diatoms derived from DPA was explained by the [Chl-a]-based model of Hirata et al. (2011b) (RMSE = 0.19, see Table 1).

Going further, we improved the regional coefficients of these polynomial models to better fit the NP pigment dataset. Table 2 presented the increasing performance estimated from the regional model and Table 3 showed the improved regional coefficients. Most of the r2 of the PFTS were increased to > 0.7, and the all the RMSE were smaller than 0.06.

3.2. Satellite validation on chlorophyll-a

Given the accuracy of underway [Chl-a] estimates(r2 = 0.95; Fig. 3), we used these high spatial resolution data for satellite matchups, to increase data coverage (shown in Fig. 9). This comparison showed reasonable agreement between in situ and satellite-derived [Chl-a] estimates, with r2 of 77% and RMSE of 0.21. However, the slope of 0.86 implied underestimation of current satellite model relative to in situ observations. Moreover, the results show that many of the satellite-derived Chl a measurements fall outside of the ± 15% band from the 1:1 line. Based on our error propagation exercise (see Section 2.5), this level of uncertainty in [Chl-a] would lead to an error of around 30% in PSCs/PFTs estimates. Thus, while the satellites appear to capture a large-scale regional trends in [Chl-a], significant errors in PSCs/PFTs may result from satellite Chla observations.

4. Discussion

Our work contributes to the growing application of optical measurements quantifying PSCs/PFTs in the ocean. In a relatively recent review, Brewin et al. (2011) compared PSCs and PFTs estimates from nine satellite-based bio-optical models against HPLC-based oceanic field measurements. This study focused on dominant phytoplankton groups, with the majority of data from Atlantic Ocean, and almost no observations from the North Pacific. The results showed that a [Chl-a]-based approach provided slightly better estimation of PSCs than other methods. Our study broadens the scope of this comparison by evaluating the ability of ship-board IOP measurements to yield both PSCs and PFTs estimates in the Subarctic Pacific Ocean. Direct ship-board measurements of IOPs circumvent uncertainties from atmospheric correction associated with satellite-based observations, and the largest source of potential error thus results from uncertainties in the optical models used to estimate PSCs/PFTs. Our new field observations provide an opportunity to evaluate the performance of four different algorithms for estimating PFTs in the Subarctic Pacific. To our knowledge, there have been no prior studies that have focused on this ocean region using optical properties to estimate PSCs/PFTs. Our work demonstrates that the simplest of the four algorithms, based only on total [Chl-a], is able to reasonably reproduce the size structure (micro%, nano% and pico%) of phytoplankton assemblages, and the relative biomass of major taxonomic groups. This provides significant new capabilities to examine the spatial and temporal patterns in phytoplankton group biomass in the Subarctic Pacific.

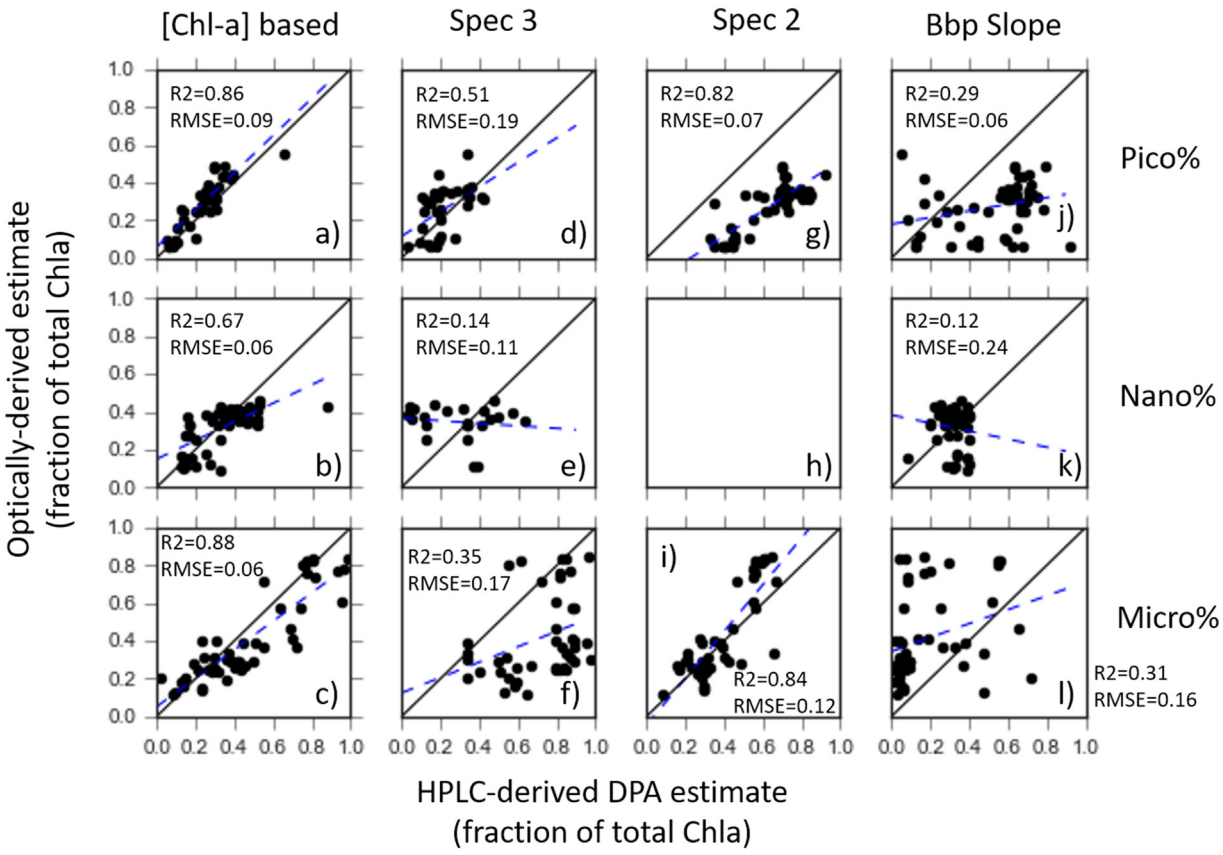

Fig. 6. HPLC-based estimates of PSCs versus estimates derived using, the Chl-a abundance approach, n = 55 (Hirata et al., 2011b)), panels (a–c); three end-member spectral decomposition approach (3 PSCs), n = 48 (Zhang et al., 2013), panels d - f; two end member spectral fitting approach (2 PSCs), n = 46 (Zhang et al., 2015), panels g - i; and b_{bp} slope approach, n = 57 (Kostadinov et al., 2009), panels j - l. RMSE is the root mean square error.

4.1. Uncertainties of DPA approach

One of the main contributions of our study is the direct comparison of PSCs values calculated from four phytoplankton size algorithms to values derived from discrete HPLC pigment analysis. In examining the results of four comparisons, it is important to understand several potential limitations of the DPA approach for estimating phytoplankton size distributions. Prior studies have suggested that DPA may not reflect true size information because some phytoplankton functional groups span more than one size class (Hirata et al., 2009, 2008; Ras et al., 2008). For example, some diatom species (e.g., *Thalassiosira pseudonana* (Mock et al., 2008)) fall into the nano-phytoplankton, rather than the micro-phytoplankton, size class. Moreover, some diagnostic pigments are shared by several phytoplankton groups (Hirata et al., 2011b). For example, fucoxanthin (fuco), which is considered as a diagnostic pigment for diatoms, is also produced in significant quantities by other phytoplankton groups such as Prymnesiophytes. Further, different light/nutrient conditions will change cellular pigment concentrations and ratios (Obayashi et al., 2001). All of these factors increase uncertainties associated with categorizing the phytoplankton size

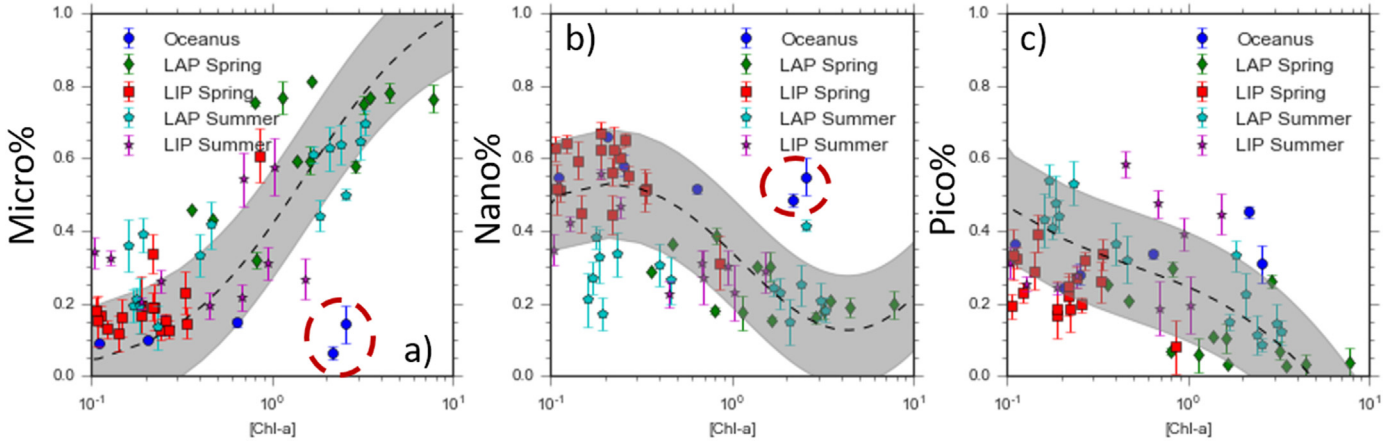

Fig. 7. The relationship between measured [Chl-a] and micro% (panel a), nano% (panel b) and pico% (panel c) from cruises conducted in 2017. Data points with error bars (± std. dev.) show direct field measurements, while the dashed line and grey patch show the predicted value and ± 15% error band of the Hirata et al. (2011b) model. Different symbols denote separate cruises, with LAP and LIP denoting La Perouse and Line P, respectively.

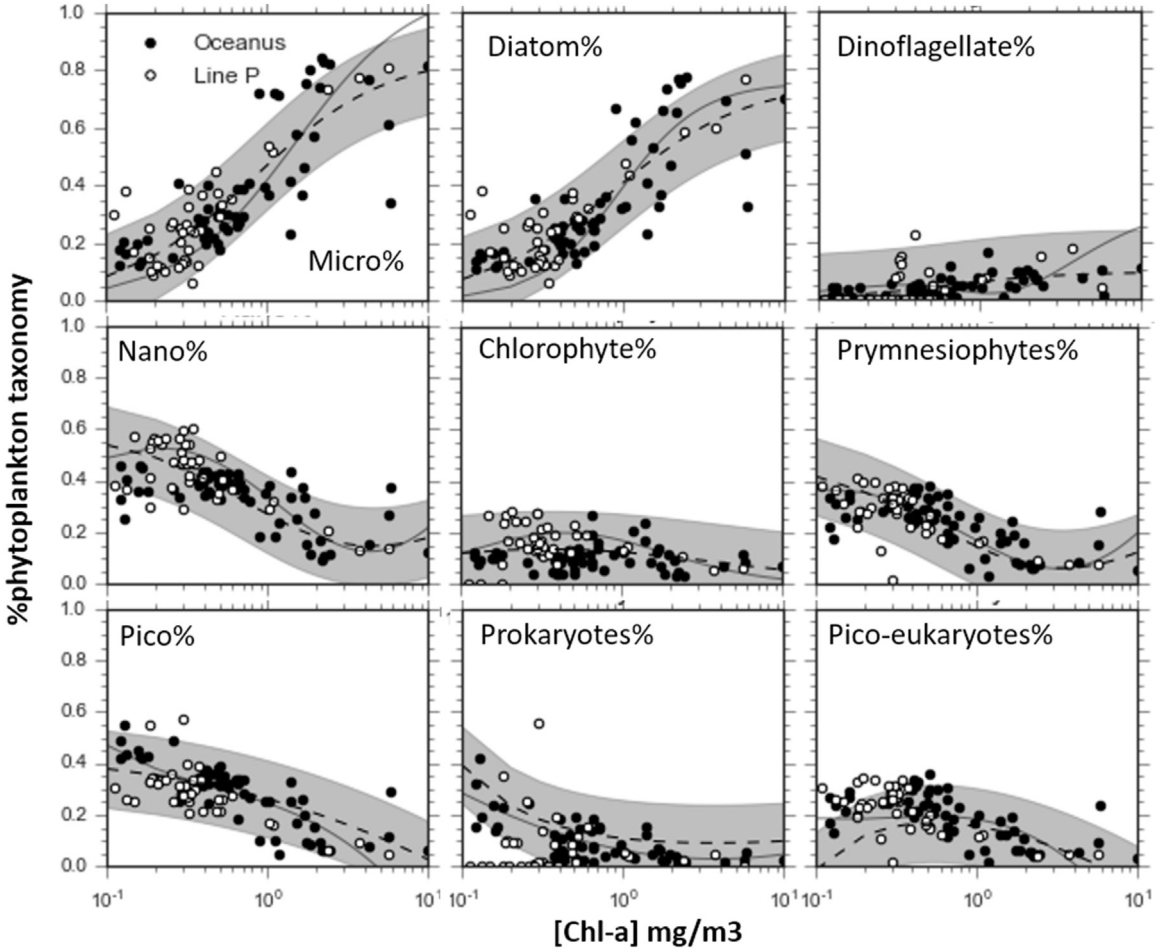

Fig. 8. [Chl-a]-based estimates of phytoplankton group biomass. Symbols represent the estimates based on DPA analysis (DPA model in Table 1) of discrete HPLC samples collected from both 2007–2011 Line P (white points) and 2016 Oceanus (black points), n = 108. Grey solid lines are polynomial model from [Chl-a] based model in Table 1). Dashed lines are improved NP model derived from region-specific tuning of algorithm coefficients (Table 3) and grey areas represent the ± 15% confidence interval of regionally-tuned polynomial model.

Table 2
Statistics of [Chl-a]-based model estimations of phytoplankton taxonomy.

Phytoplankton Groups	r^2	RMSE*	Improved r^2	Improved RMSE*
Micro%	0.86	0.059	0.86	0.044
Nano%	0.30	0.08	0.76	0.052
Pico%	0.70	0.095	0.80	0.047
Diatom%	0.86	0.055	0.86	0.045
Dinoflagellat%	0.29	0.112	0.50	0.042
Chlorophyte%	0.20	0.069	0.30	0.030
Prymnesiophte%	0.30	0.303	0.72	0.054
Prokaryotes%	0.32	0.061	0.45	0.055
Pico-eukaryotes%	0.50	0.117	0.74	0.037

*RMSE is the root mean square between DPA derived and [Chl-a] based PFTs/PSCs.

distributions by pigment analysis. However, DPA is still considered the most efficient and effective current approach to classify phytoplankton taxonomy biomass based on historical pigment measurements (Hirata et al., 2011b).

In addition, we compared DPA with CHEMTAX estimated micro%, and found that both produced similar trends of micro% but with much lower values (data not shown). The apparent discrepancy may result from the sensitivity of the CHEMTAX results to the initial starting pigment matrix used in the iterative calculations. In our analysis, we used a single starting pigment matrix, derived from Table 5 in Lee et al. (2011). However, given that we transected a number of distinct oceanographic regimes (e.g. low productivity HNLC vs. high productivity coastal upwelling), the analysis would likely have needed a number of different starting pigment matrices to produce the best results. Moreover, the CHEMTAX and DPA estimate different phytoplankton classes, so that those two methods cannot be directly compared. We thus chose to focus on DPA analysis, which compares more directly with the work of Hirata et al. (2011b) and others.

Additional measurements of size-fractionated [Chl-a] can also be used to provide a simple and relatively unambiguous estimate of phytoplankton size structure. Our results (Fig. 7) indicate that the Hirata et al. (2011b) model is able to capture trends in phytoplankton size class biomass. In future work, simultaneous deployment of single-cell imaging systems such as FlowCam could be employed to obtain more nuanced estimates of phytoplankton assemblage size structure, to further improve algorithm validation.

Our assessment of the potential sensitivity of the DPA approach to the uncertainties in input pigment composition show that 5% variability in input pigment concentrations produces errors of 5%, 7%, and 10% for micro%, nano% and pico% estimates, respectively. Increasing the magnitude of pigment variation to 15% yields uncertainties of 20%, 25% and 30% for micro%, nano% and pico%, respectively. The pico% estimation is least robust because the relative biomass of this group in our study region never exceeded ~ 50% of the total [Chl-a]. Results from our error propagation model imply that the model error from [Chl-a] based approach is acceptable since HPLC and DPA measurements produce at least 5% error in PSCs.

Table 3
Coefficients and formulas for global (G) and regional North Pacific (NP) [Chl-a] based approach. Values for the global coefficients are derived from Hirata et al. (2011b), while regional coefficients were derived from a least-square fit to the data collected in this study.

PSCs/PFTs	Chl-a based approach[a]	T[b]	A0	A1	A2	A3	A4	A5	A6
Micro-plankton	$[a0+\exp(a1x+a2)]^{-1}$	G[c]	0.912	− 2.733	0.400				
		NP[d]	1.172	− 2.423	− 0.035				
Diatom	$[a0+\exp(a1x+a2)]^{-1}$	G	1.327	− 3.983	0.195				
		NP	1.317	− 2.388	0.129				
Dinoflagellate	Micro-Diatom								
Nano-plankton	1-Micro-Nano								
Chlorophyte	$(a0/y)\exp[(a1x+a2)^2]$	G	0.249	− 1.2621	− 0.552				
		NP	1.112	− 0.418	− 2.290				
Prymnesio-phytes	Nano-Chlorophyte								
Pico-plankton	$-[a0+\exp(a1x+a2)]^{-1}+a3x+a4$	G	0.153	1.031	− 1.558	− 1.860	3.0		
		NP	− 0.061	− 0.112	− 1.293	0.503	4.947		
Prokaryotes	$\left(\frac{\frac{a0}{a1}}{y}\right)\exp\left[\frac{a2(x+a3)^2}{a1^2}\right]+a4x^2+a5x+a6$	G	0.007	0.616	− 19.519	− 1.86	0.103	− 0.119	0.0626
		NP	− 0.253	− 8.154	− 17.3	1.214	− 0.02	0.004	0.039
Pico-eukaryotes	Pico-Prokaryotes								

[a] x:log10(Chl-a);y:Chl-a
[b] Type of model.
[c] Global
[d] North Pacific

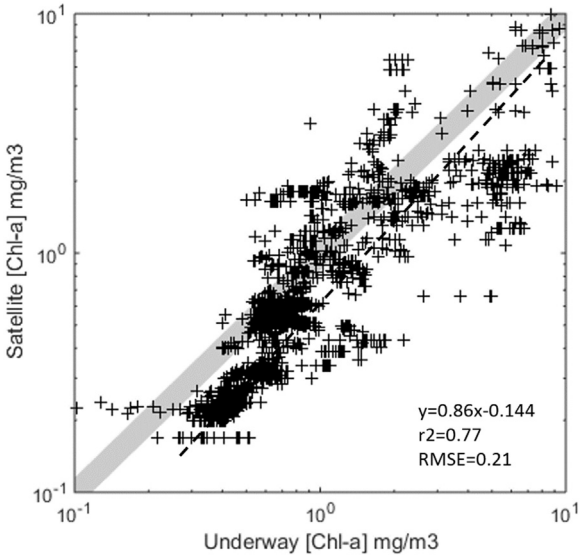

Fig. 9. Comparison between underway ship-board and satellite derived [Chl-a], grey area showed the ± 15% of the 1:1line.

Another source of uncertainty in using the model of Hirata et al. (2011b) is the assumption that the seven diagnostic pigments (Σ DP), weighted by an empirical regression, sum to total [Chl-a] (Uitz et al., 2006; Vidussi et al., 2001). In our analysis, we found that Σ DP values from the HPLC pigment analyses in the Subarctic North Pacific were lower than [Chl-a] measured by HPLC analysis. However, normalizing the biomass of each group by Σ DP decreases the absolute discrepancy between Σ DP and total [Chl-a], and does not affect estimates of phytoplankton taxonomic biomass by DPA (Fig. 8) (Hirata et al., 2011b). Our results (Table 3) show that further improvements can be achieved by specifically tuning the DPA model to the Subarctic Pacific. For example, despite being one of the few taxonomic groups with a unique diagnostic pigment (allo), cryptophytes were not included in the Hirata et al. (2011b) algorithm due to low allo concentrations in their dataset. However, microscopy data indicates cryptophytes are abundant in many of the coastal samples from the Line P archive. We found that the use of regionally derived coefficients for the model significantly increased its predictive power over that derived from the global study of Hirata et al. This result supports the development of regionally-tuned versions of the Hirata et al. (2011b) model.

4.2. Comparisons between 4 algorithms on phytoplankton taxonomy

We found clear differences in the ability of the four algorithms (Chl-a based, two end-member spectral fitting, three member spectral decomposition and b_{bp}-slope) to estimate PSCs/PFTs. The poorest results were obtained with the b_{bp} slope algorithm, and there are three potential reasons for this result. First, the b_{bp} slope is calculated from only three wavelengths, and is thus expected to have significant uncertainty, since the slope is highly sensitive to any of the three data points which are required (as a minimum) for the exponential slope regression. The presence of small bubbles near one or more of the detectors could thus exert significant influence on the resulting slope estimates. Secondly, Kostadinov et al. (2009) constructed the look-up table based on satellite measuring channels with rather narrow band widths (± 10 nm) and short bands span (490, 510, 550 nm), while our BB3 measurements were made using a 20 nm band width and long bands span (470, 532, 650 nm). Wide band width reduces variability in the measurements and long band (eg. 650 nm) produces weak signal, those will act to increase noise in the resulting back scatter data in our case, likely influencing the derived wavelength dependence. A further potential for the poor performance of the back-scatter slope approach is the fact that estimates of b_{bp} slope and particle size distributions (PSD) are based on Mie theory, which assumes normally distributed homogeneous particles. With this approach, the b_{bp} signals are calculated as the integral of scattering by phytoplankton cells only. However, it is likely that NAPs and various mineral phases (e.g. calcite) contribute significantly to the b_{bp} signal in coastal regions of the Subarctic Pacific, and thus cannot be neglected in the PSD estimation. For instance, the presence of calcified coccolithophores has been documented in a number of Subarctic regions (Beaufort et al., 2008; Peterson et al., 2007), and these cells would have a strong backscatter signal that would not be accounted for using the Mie theory approach. Coccolithophores are commonly observed throughout the Subarctic Pacific during summer, and we did see evidence for calcite in surface waters based on remote sensing observations from the AquaModis sensor (data not shown).

The two end-member spectrum fitting approach also has potential limitations. For example, shifts in phytoplankton pigment ratios and cell sizes (Obayashi et al., 2001) in response to light and nutrient variability could alter absorption spectra, complicating the choice of

end-members for estimating PSCs. The separation of a_{ph} and a_{NAP} (Eqs. 4–6) is a fundamental step of the spectrum fitting approach. In low productivity open ocean waters, the shape of a_{NAP} is relatively well constrained (Zhang et al., 2013). In contrast, the higher biomass of suspended particulate matter in coastal waters may complicate the determination of a_{NAP}, and thus the separation of algal and non-algal absorption signatures. In the case of the three end-member spectral decomposition approach, the use of a uniform wavelength-dependence for a_{CDOM} could be problematic in a highly dynamics region, such as the coastal NAP, with significant variability in nutrient levels, productivity and dissolved organic matter.

Given the uncertainties in the b_{bp} slope and spectrum fitting algorithms, and because the [Chl-a] algorithm yielded the good agreement with HPLC-derived PSCs values (Fig. 6), HPLC-derived PFTs (Fig. 8) and size fractioned [Chl-a] PSCs (Fig. 7), we argue for use of the [Chl-a] algorithm in future studies. This algorithm is mathematically simple, requiring significantly less computation than the non-linear spectrum fitting approach, and it also provides information on the relative biomass of different phytoplankton groups (Hirata et al., 2011b). Indeed, we found that the Hirata et al. (2011b) algorithm performed well in reconstructing phytoplankton community composition measured by HPLC pigment analysis. This was particularly true for highly abundant groups, such as diatoms and prymnesiophytes, which are important to the productivity and biogeochemical cycles of the Subarctic Pacific (Peña and Varela, 2007).

Despite the good performance of the Hirata et al. (2011b) algorithm in our data set, there are several potential caveats to consider in the application of this model. First, it is important to note that the robustness of the [Chl-a] based approach diminishes beyond 10 mg Chl-a m^{-3}. Model simulations of polynomial functions relating community structure to trophic level in Hirata et al. (2011b) (indexed by [Chl-a]) show significant errors due to polynomial swing. More validations beyond this [Chl-a] value in the field will likely help to improve the fit. Additional validations with taxonomic estimations based on microscopy (Peña and Varela, 2007) or 18 s rRNA (Moon-van der Staay et al., 2000) would also be useful. In applying such approaches, however, it important to move beyond simple abundance estimates, incorporating information on cell sizes to yield estimates of relative biomass contributions of different groups. In this respect, it is important to note that the classification of phytoplankton into discrete groups, micro%, nano % and pico%, do not provide information on the full continuous size spectrum present in surface ocean waters. Further, the [Chl-a] approach is subject to variability resulting from changes in cellular Chl-a quotas or C: Chl-a ratios. In our recent work, for example, we documented significant variability in C: Chl-a ratios across the Subarctic Pacific, with values ranging from 50 to 400 (Burt et al., 2018). This variability appears to be driven primarily by light intensity and nutrient limitation, and implies a decoupling between [Chl-a] and the biomass of various plankton groups.

4.3. Conclusions and Future directions

Our results show that underway measurements of [Chl-a] can yield high-resolution estimates of phytoplankton biomass, size distribution, and community composition throughout the Subarctic Pacific Ocean. Such measurements can be used to quantify the biomass of important phytoplankton groups like diatoms, prokaryotes and prymnesiophytes within uncertainties of ± 15% after applying regional coefficients. We also validated PSCs estimations against size-fractioned [Chl-a] measurements (Fig. 7). Looking forward, we suggest that this approach can be applied to satellite-derived [Chl-a] to examine changes in phytoplankton PSCs/PFTs in the Subarctic Pacific over large spatial and temporal scales. This work will, however, require continued improvement of satellite [Chl-a] estimates. At present, satellite products in the Subarctic Pacific contain uncertainties due to an uneven distribution in field-based validation samples. In addition, current satellite-derived [Chl-a] values calculated using the Ocean Color OCI algorithm (O'Reilly et al., 2000; https://oceancolor.gsfc.nasa.gov/reprocessing/r2009/ocv6) show an uncertainty > 15% against in situ [Chl-a] in this region (Fig. 9). This uncertainty will cause at least 20% of error in micro % and more than 30% of error in pico% estimation. More work is thus needed before PSCs/PFTs can be derived with confidence from remote sensing observations. Continued deployment of autonomous ship-board optical sensors, such as the system described here, will expand the database available for the improvement and regional tuning of satellite products, leading to improved estimates phytoplankton size class and functional type biomass over synoptic scales. Such information will be critical to better understanding marine ecological response to short-term environmental perturbations, including sporadic iron fertilization events, and climate forcing on various time-scales, from El Nino cycles to decadal-scale warming and acidification.

Acknowledgements

We thank the officers and crew of the *CCGS John P. Tully* and *R/V Oceanus* for their help during the cruises. This work was supported by China Scholarship Council (CSC201506260127) and by the Natural Sciences and Engineering Research Council of Canada. In addition, we appreciated the fund from the State Key Program of National Natural Science of China (Grant No. 41530960) and the Chinese Polar Environment Comprehensive Investigation & Assessment Programmes (Grant no. CHINARE2017-02-04).

References

Aiken, J., Hardman-Mountford, N.J., Barlow, R., Fishwick, J., Hirata, T., Smyth, T., 2008. Functional links between bioenergetics and bio-optical traits of phytoplankton taxonomic groups: an overarching hypothesis with applications for ocean colour remote sensing. J. Plankton Res. 30, 165–181. http://dx.doi.org/10.1093/plankt/fbm098.

Alvain, S., Moulin, C., Dandonneau, Y., Bréon, F.M., 2005. Remote sensing of phytoplankton groups in case 1 waters from global SeaWiFS imagery. Deep. Res. Part I Oceanogr. Res. Pap. 52, 1989–2004. http://dx.doi.org/10.1016/j.dsr.2005.06.015.

Armstrong, R.A., Lee, C., Hedges, J.I., Honjo, S., Wakeham, S.G., 2002. A new, mechanistic model for organic carbon fluxes in the ocean based on the quantitative association of POC with ballast minerals. Deep. Res Part II 49, 219–236.

Beaufort, L., Couapel, M., Buchet, N., Claustre, H., Goyet, C., 2008. Calcite production by coccolithophores in the south east Pacific Ocean. Biogeosciences 5, 1101–1117. http://dx.doi.org/10.5194/bg-5-1101-2008.

Bélanger, S., Cizmeli, S.A., Ehn, J., Matsuoka, A., Doxaran, D., Hooker, S., Babin, M., 2013. Light absorption and partitioning in Arctic Ocean surface waters: impact of multiyear ice melting. Biogeosciences 10, 6433–6452. http://dx.doi.org/10.5194/bg-10-6433-2013.

Booth, B.C., Lewin, J., Postel, J.R., 1993. Temporal variation in the structure of autotrophic and heterotrophic communities in the sub-arctic pacific. Prog. Oceanogr. 32, 57–99. http://dx.doi.org/10.1016/0079-6611(93)90009-3.

Bouman, H., Platt, T., Sathyendranath, S., Stuart, V., 2005. Dependence of light-saturated photosynthesis on temperature and community structure. Deep. Res. Part I Oceanogr. Res. Pap. 52, 1284–1299. http://dx.doi.org/10.1016/j.dsr.2005.01.008.

Brewin, R.J.W., Hardman-Mountford, N.J., Lavender, S.J., Raitsos, D.E., Hirata, T., Uitz, J., Devred, E., Bricaud, A., Ciotti, A., Gentili, B., 2011. An intercomparison of bio-optical techniques for detecting dominant phytoplankton size class from satellite remote sensing. Remote Sens. Environ. 115, 325–339. http://dx.doi.org/10.1016/j.rse.2010.09.004.

Bricaud, A., Claustre, H., Ras, J., Oubelkheir, K., 2004. Natural variability of phytoplanktonic absorption in oceanic waters: influence of the size structure of algal populations. J. Geophys. Res. Ocean. 109, 1–12. http://dx.doi.org/10.1029/2004JC002419.

Bricaud, A., Stramski, D., 1990. Spectral absorption coefficients of living phytoplankton and nonalgal biogenous matter: a comparison between the Peru upwelling area and the Sargasso Sea. Limnol. Oceanogr. 35, 562–582. http://dx.doi.org/10.4319/lo.1990.35.3.0562.

Buesseler, K.O., 1998. The decoupling of production and particle export in the surface ocean. Glob. Biogeochem. Cycles 12, 297–310. http://dx.doi.org/10.1029/97GB03366.

Burt, J.B., Westberry, T.K., Behrenfeld, M.J., Zeng, Z., Izett, R., Tortell, P.D., 2018. Carbon: chlorophyll ratios and net primary productivity of Subarctic Pacific surface waters derived from autonomous shipboard sensors. Glob. Biogeochem. Cycles 32, 267–288. http://dx.doi.org/10.1002/2017GB005783.

Caddy, J.F., Refk, R., Do-Chi, T., 1995. Productivity estimates for the Mediterranean: evidence of accelerating ecological change. Ocean Coast. Manag. 26, 1–18. http://dx.doi.org/10.1016/0964-5691(95)00015-T.

Ciotti, A.M., Lewis, M.R., Cullen, J.J., 2002. Assessment of the relationships between

dominant cell size in natural phytoplankton communities and the spectral shape of the absorption coefficient. Limnol. Oceanogr. 47, 404–417. http://dx.doi.org/10.4319/lo.2002.47.2.0404.

Dall'Olmo, G., Boss, E., Behrenfeld, M.J., Westberry, T.K., 2012. Particualte optical scattering coefficents along an Atlantic meridional transect. Opt. Express 20, 1–20. http://dx.doi.org/10.1029/2004GB002299.

Francois, R., Honjo, S., Krishfield, R., Manganini, S., 2002. Factors controlling the flux of organic carbon to the bathypelagic zone of the ocean. Glob. Biogeochem. Cycles 16, 1087. http://dx.doi.org/10.1029/2001gb001722.

Harrison, P.J., Boyd, P.W., Varela, D.E., Takeda, S., Shiomoto, A., Odate, T., 1999. Comparison of factors controlling phytoplankton productivity in the NE and NW subarctic Pacific gyres. Prog. Oceanogr. 43, 205–234. http://dx.doi.org/10.1016/S0079-6611(99)00015-4.

Harrison, P.J., Whitney, F.A., Tsuda, A., Saito, H., Tadokoro, K., 2004. Nutrient and plankton dynamics in the NE and NW gyres of the subarctic Pacific Ocean. J. Oceanogr. 60, 93–117. http://dx.doi.org/10.1023/B:JOCE.0000038321.57391.2a.

Hirata, T., Aiken, J., Hardman-Mountford, N., Smyth, T.J., Barlow, R.G., 2008. An absorption model to determine phytoplankton size classes from satellite ocean colour. Remote Sens. Environ. 112, 3153–3159. http://dx.doi.org/10.1016/j.rse.2008.03.011.

Hirata, T., Hardman-Mountford, N.J., Barlow, R., Lamont, T., Brewin, R., Smyth, T., Aiken, J., 2009. An inherent optical property approach to the estimation of size-specific photosynthetic rates in eastern boundary upwelling zones from satellite ocean colour: an initial assessment. Prog. Oceanogr. 83, 393–397. http://dx.doi.org/10.1016/j.pocean.2009.07.019.

Hirata, T., Hardman-Mountford, N.J., Brewin, R.J.W., Aiken, J., Barlow, R., Suzuki, K., Isada, T., Howell, E., Hashioka, T., Noguchi-Aita, M., Yamanaka, Y., 2011a. Synoptic relationships between surface Chlorophyll-a and diagnostic pigments specific to phytoplankton functional types. Biogeosciences 8, 311–327. http://dx.doi.org/10.5194/bg-8-311-2011.

Hirata, T., Hardman-Mountford, N.J., Brewin, R.J.W., Aiken, J., Barlow, R., Suzuki, K., Isada, T., Howell, E., Hashioka, T., Noguchi-Aita, M., Yamanaka, Y., 2011b. Synoptic relationships between surface chlorophyll-a and diagnostic pigments specific to phytoplankton functional types. Biogeosciences 8, 311–327. http://dx.doi.org/10.5194/bg-8-311-2011.

Klaas, C., Archer, D.E., 2002. Association of sinking organic matter with various types of mineral ballast in the deep sea: implications for the rain ratio. Glob. Biogeochem. Cycles 16, 1–14. http://dx.doi.org/10.1029/2001GB001765.

Kostadinov, T.S., Siegel, D.A., Maritorena, S., 2009. Retrieval of the particle size distribution from satellite ocean color observations. J. Geophys. Res. Ocean. 114, 1–22. http://dx.doi.org/10.1029/2009JC005303.

Lee, Y., Park, M., Kim, Y., Kim, S., Kang, C., 2011. Application of photosynthetic pitment analysis using a HPLC and CHEMTAX program to studies of phytplankton community composition. J. Korean Soc. Oceanogr. 16, 117–124.

Lin, J., Cao, W., Zhou, W., Sun, Z., Xu, Z., Wang, G., Hu, S., 2014. Novel method for quantifying the cell size of marine phytoplankton based on optical measurements. Opt. Express 22, 10467. http://dx.doi.org/10.1364/OE.22.010467.

Mackey, M.D., Mackey, D.J., Higgins, H.W., Wright, S.W., 1996. CHEMTAX - A program for estimating class abundances from chemical markers: application to HPLC measurements of phytoplankton. Mar. Ecol. Prog. Ser. 144, 265–283. http://dx.doi.org/10.3354/meps144265.

Michaels, A.F.A.M.W.S., 1988. Primary production, sinking fluxes and the microbial food web. Deep. Res. 35, 473–490.

Mitchell, B.G., 1990. Algorithms for determining the absorption coefficient of aquatic particulates using the quantitative filter technique (QFT). Ocean Opt. 1302, 137–148.

Mock, T., Samanta, M.P., Iverson, V., Berthiaume, C., Robison, M., Holtermann, K., Durkin, C., Bondurant, S.S., Richmond, K., Rodesch, M., Kallas, T., Huttlin, E.L., Cerrina, F., Sussman, M.R., Armbrust, E.V., 2008. Whole-genome expression profiling of the marine diatom Thalassiosira pseudonana identifies genes involved in silicon bioprocesses. Proc. Natl. Acad. Sci. Usa. 105, 1579–1584. http://dx.doi.org/10.1073/pnas.0707946105.

Moon-van der Staay, S.Y., van der Staay, G.W.M., Guillou, L., Vaulot, D., Claustre, H., Medlin, L.K., 2000. Abundance and diversity of prymnesiophytes in the picoplankton community from the equatorial Pacific Ocean inferred from 18S rDNA sequences. Limnol. Oceanogr. 45, 98–109. http://dx.doi.org/10.4319/lo.2000.45.1.0098.

Nelson, N.B., Prezelin, B.B., Bidigare, R.R., 1993. Phytoplankton light absorption and the package effect in California coastal waters. Mar. Ecol. Prog. Ser. 94, 217–227. http://dx.doi.org/10.3354/meps094217.

Nemcek, N., Pena, M.A., 2014. Institute of Ocean sciences protocols for phytoplankton pigment analysis by HPLC. Can. Tech. Report. Fish. Aquat. Sci. 3117.

O'Reilly, J.E., Maritorena, S., O'Brien, M.C., Siegel, D. a., Toole, D., Menzies, D., Smith, R.C., Mueller, J.L., Mitchell, B.G., Kahru, M., Chavez, F.P., Strutton, P., Cota, G.F., Hooker, S.B., Mcclain, C.R., Carder, K.L., Müller-Karger, F.E., Harding, L., Magnuson, A., Phinney, D., Moore, G.F., Aiken, J., Arrigo, K.R., Letelier, R., Culver, M., 2000. SeaWiFS Postlaunch Calibration and validation analyses, Part 3. SeaWiFS Postlaunch tech. Rep. Ser. 11 (51pp).

Obayashi, Y., Tanoue, E., Suzuki, K., Handa, N., Nojiri, Y., Wong, C.S., 2001. Spatial and temporal variabilities of phytoplankton community structure in the northern North Pacific as determined by phytoplankton pigments. Deep. Res. Part I-Oceanogr. Res. Pap. 48, 439–469. http://dx.doi.org/10.1016/S0967-0637(00)00036-4.

Organelli, E., Bricaud, A., Antoine, D., Uitz, J., 2013. Multivariate approach for the retrieval of phytoplankton size structure from measured light absorption spectra in the Mediterranean Sea (BOUSSOLE site)52.

Parsons, T.R., Lalli, C.M., 2002. Jellyfish population explosions: Revisiting a hypothesis of possible causes. Mer. https://doi.org/111-121.

Pegau, S., Zaneveld, J.R. V, Mitchell, B.G., Mueller, J.L., Kahru, M., Wieland, J., Stramska, M., 2002. Ocean optics protocols for satellite ocean color sensor validation, Revision 4, Volume IV: Inherent optical properties: instruments, characterizations, field measurements and data analysis protocols. Ocean Color web page IV, 76.

Peña, M.A., Varela, D.E., 2007. Seasonal and interannual variability in phytoplankton and nutrient dynamics along Line P in the NE subarctic Pacific. Prog. Oceanogr. 75, 200–222. http://dx.doi.org/10.1016/j.pocean.2007.08.009.

Peterson, T.D., Toews, H.N.J., Robinson, C.L.K., Harrison, P.J., 2007. Nutrient and phytoplankton dynamics in the Queen Charlotte Islands (Canada) during the summer upwelling seasons of 2001–2002. J. Plankton Res. 29, 219–239. http://dx.doi.org/10.1093/plankt/fbm010.

Platt, T., Bouman, H., Devred, E., Fuentes-Yaco, C., Sathyendranath, S., 2005. Physical forcing and phytoplankton distributions. Sci. Mar. 69, 55–73. http://dx.doi.org/10.3989/scimar.2005.69s155.

Platt, T., Denman, K., 1977. Organisation in the pelagic ecosystem. Helgoländer Wissenschaftliche Meeresuntersuchungen 30, 575–581. ⟨https://doi.org/10.1007/BF02207862⟩.

Ras, J., Claustre, H., Uitz, J., 2008. Spatial variability of phytoplankton pigment distributions in the Subtropical South Pacific Ocean: comparison between in situ and predicted data. Biogeosciences 5, 353–369. http://dx.doi.org/10.5194/bgd-4-3409-2007.

Roesler, C.S., Barnard, A.H., 2013. Optical proxy for phytoplankton biomass in the absence of photophysiology: rethinking the absorption line height. Methods Oceanogr. 7, 79–94. http://dx.doi.org/10.1016/j.mio.2013.12.003.

Siegenthaler, U., Sarmiento, J.L., 1993. Atmospheric carbon dioxide and the ocean. Nature 365, 119–125. http://dx.doi.org/10.1038/365119a0.

Slade, W.H., Boss, E., Dall'olmo, G., Langner, M.R., Loftin, J., Behrenfeld, M.J., Roesler, C., Westberry, T.K., 2010. Underway and moored methods for improving accuracy in measurement of spectral particulate absorption and attenuation. J. Atmos. Ocean. Technol. 27, 1733–1746. http://dx.doi.org/10.1175/2010JTECHO755.1.

Twardowski, M.S., Claustre, H., Freeman, S.A., Stramski, D., Huot, Y., 2007. Optical backscattering properties of the "clearest" natural waters. Biogeosciences Discuss 4. pp. 2441–2491. http://dx.doi.org/10.5194/bgd-4-2441-2007.

Uitz, J., Claustre, H., Morel, A., Hooker, S.B., 2006. Vertical distribution of phytoplankton communities in open ocean: an assessment based on surface chlorophyll. J. Geophys. Res. Ocean. 111. http://dx.doi.org/10.1029/2005JC003207.

Uitz, J.U., Huot, Y., Bruyant, F., Babin, M., Claustre, H., 2008. Relating phytoplankton photophysiological properties to community structure on large scales. Limnol. Oceanogr. 53, 614–630. http://dx.doi.org/10.4319/lo.2008.53.2.0614.

Van Heukelem, L., Thomas, C.S., 2001. Computer-assisted high-performance liquid chromatography method development with applications to the isolation and analysis of phytoplankton pigments. J. Chromatogr. A 910, 31–49. http://dx.doi.org/10.1016/S0378-4347(00)00603-4.

Vidussi, F., Claustre, H., Manca, B.B., Luchetta, A., Marty, J.-C., 2001. Phytoplankton pigment distribution in relation to upper thermocline circulation in the eastern Mediterranean Sea during winter. J. Geophys. Res. Ocean. 106, 19939–19956. http://dx.doi.org/10.1029/1999JC000308.

Waterbury, J.B., Watson, S.W., Guillard, R.R.L., Brand, L.E., 1979. Widespread occurance of a unicellular, marine, planktonic, cyanobacterium. Nature.

Xi, H., Hieronymi, M., Röttgers, R., Krasemann, H., Qiu, Z., 2015. Hyperspectral differentiation of phytoplankton taxonomic groups: a comparison between using remote sensing reflectance and absorption spectra. Remote Sens. 7, 14781–14805. http://dx.doi.org/10.3390/rs71114781.

Zhang, X., Huot, Y., Bricaud, A., Sosik, H.M., 2015. Inversion of spectral absorption coefficients to infer phytoplankton size classes, chlorophyll concentration, and detrital matter. Appl. Opt. 54, 5805. http://dx.doi.org/10.1364/AO.54.005805.

Zhang, X., Huot, Y., Gray, D.J., Weidemann, A., Rhea, W.J., 2013. Biogeochemical origins of particles obtained from the inversion of the volume scattering function and spectral absorption in coastal waters. Biogeosciences 10, 6029–6043. http://dx.doi.org/10.5194/bg-10-6029-2013.

Zubkov, M.V., Sleigh, M.A., Burkill, P.H., Leakey, R.J.G., 2000. Picoplankton community structure on the Atlantic Meridional Transect: a comparison between seasons. Prog. Oceanogr. 45, 369–386. http://dx.doi.org/10.1016/S0079-6611(00)00008-2.

Zubkov, M.V., Fuchs, B.M., Tarran, G.A., Burkill, P.H., Amann, R., 2003. High rate of uptake of organic nitrogen compounds by Prochlorococcus cyanobacteria as a key to their dominance in oligortrophic oceanic waters. Appl. Environ. Microbiol. 69, 1299–1304. http://dx.doi.org/10.1128/AEM.69.2.1299.